10th ANKARA INTERNATIONAL AEROSPACE CONFERENCE AIAC-2019-117
18-20 September 2019 - METU, Ankara TURKEY

DEVELOPMENT OF A PRELIMINARY ESTIMATION CODE FOR NON-CHARRING ABLATION OF METALLIZED SOLID PROPELLANT ROCKET MOTOR NOZZLES

Mehmet Eren Dağ[1]
Middle East Technical University
Ankara, Turkey

ABSTRACT

Nozzle is an integral part of the rocket propulsion system. Therefore, its design depends on input variables from combustion chamber, geometric envelope from vehicle requirements and operating conditions from ambient environment. During the design process, many changes may occur and quick response to these changes may be needed from different divisions since nozzle design is a multidisciplinary process in which the design should be reviewed in terms of aerodynamic, thermal and mechanical considerations. Preliminary design codes are employed in preliminary design phase to give rapid feedback to design changes during iterative nozzle design. Determination of nozzle ablation and heat transfer rates through the nozzle is the main purpose of thermal design process. Development of a preliminary thermal analysis code in order to predict chemical non-charring erosion and heat transfer is the main intention of this paper.

INTRODUCTION

During the rocket motor operation time, thermal protection systems (TPS) employed inside the nozzle are exposed to convective and radiative heat flux as well as the ablation while high-temperature, erosive gases conveyed through the nozzle contour. Estimation of nozzle recession is required to predict nozzle performance and satisfy thermal protection objectives during the motor operation period. Especially, evolution throat diameter should be considered, since it determines mass flow rate of combustion gases and therefore overall performance of rocket motor system. TPS materials are classified as charring and non-charring ablators with respect to their thermochemical ablation mechanisms.

Non-charring Ablation

For non-charring ablation mechanisms, surface of the material reacts with boundary layer gases and TPS material chemically erodes into reaction products and material recession occurs. TPS materials such as graphite, C-C composites, refractory materials show this kind of ablation mechanisms when they are exposed to corrosive chamber gases.

Charring Ablation

Some composite materials used as TPS shows different ablation mechanism named as charring ablation. Charring materials absorbs the heat and decomposes into char and gas which is named as pyrolysis reaction. Since this reaction is endothermic, the amount of heat conducted across the material is reduced. During the transition of pyrolysis gas from pyrolysis zone to boundary layer, pyrolysis gas shows cooling effect on porous char layer. Moreover,

[1] M. Sc Student in Aerospace Engineering,METU Email: erendag@ae.metu.edu.tr

when it reaches the boundary layer, it decreases the convection heat transfer from the boundary layer of the fluid. Phenolic resins with different type of fibres such as carbon, silica, polyester etc. are employed as TPS inside the nozzle due to their tempting low thermal conductivity and weight. Chemical and physical mechanisms that occur for non-charring and charring reactions are given in figure 1.

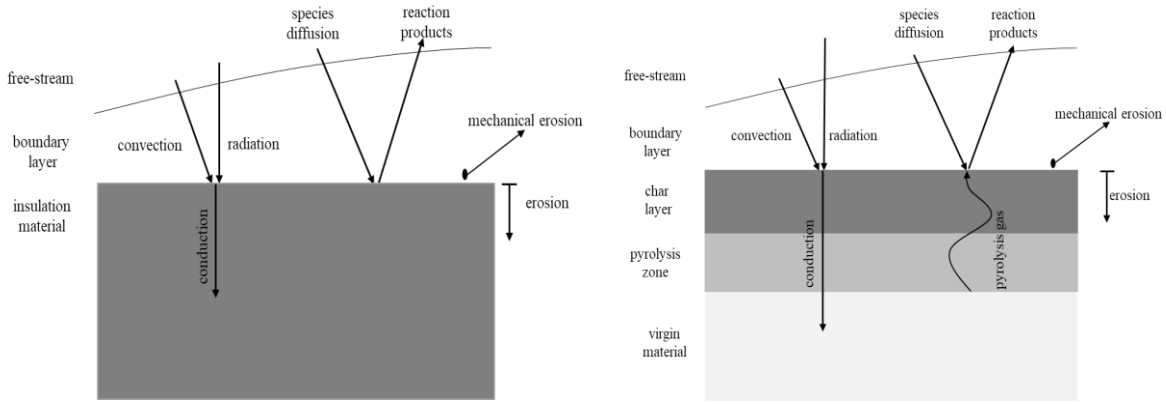

Figure 1: Non-charring (left) and charring (right) ablation mechanisms.

Non-charring Ablation Mechanism

TPS employed in nozzle is heated by convection and radiation from the combustion products. Heat flux is conducted by nozzle material. However, elevation of temperature of nozzle material provides necessary energy for reaction of nozzle material with the hot gases. The reaction of combustion gases with nozzle material is classified as heterogenous reaction since it occurs at an interface between solid and gas. [Kuo and Acharya, 2012] Diffusion of reacting gases continues through boundary layer which results gradual removal of insulation material due to chemical reactions. In addition, high shear flow results spallation of material which contributes to recession. Removal of material due to shear forces is called mechanical erosion.

If the reaction of TPS material with gases is faster than diffusion of oxidizing species in the boundary layer, reaction mechanism is classified as diffusion limited. On the other hand,

Reaction of metallized propellants with graphite show diffusion limited behaviour, since oxidizing species concentration in the freestream is lower. Also, temperature of TPS material interface is relatively higher due to higher combustion temperature which increases reaction rates. Reactions of graphite with H_2O, CO_2, OH, O, O_2 and NO are proven to be possible whereas reactions with H_2, Cl, HCl and N_2 are not favourable. Also, Al_2O_3 particles can be treated as an inert gas, since they exist as condensed phase in the freestream. [Thakre, 2008] Recession measurements from the experiments [Borie, Brulard and Lengelle, 1989; Geisler and Beckman, 1998] indicates that evolution of nozzle throat shows nearly linear increase during the motor operation after ignition transient period and initial heating of the TPS material.

METHOD

Nozzle inlet conditions such as pressure, temperature and mass fractions are needed as inputs to perform calculations. In order to get Mach number through variation of area, following equation is used [Sutton and Biblarz, 2001].

$$\frac{A_x}{A_y} = \frac{M_y}{M_x}\sqrt{\left\{\frac{1+[\frac{\gamma-1}{2}]M_x^2}{1+[\frac{\gamma-1}{2}]M_y^2}\right\}^{(\gamma+1)/(\gamma-1)}} \tag{1}$$

At throat, Mach number is equal to 1. Therefore, Mach number variation along the nozzle can be computed by iterating the following equation (2).

$$\frac{A_x}{A_t} = \frac{1}{M_x}\sqrt{\left\{\frac{1+[\frac{\gamma-1}{2}]M_x^2}{1+[\frac{\gamma-1}{2}]}\right\}^{(\gamma+1)/(\gamma-1)}} \tag{2}$$

Pressure and temperature can be calculated with isentropic relations as below.

$$P = \frac{P_{cc}}{[1+\frac{(\gamma-1)}{2}M^2]^{\gamma/(\gamma-1)}} \tag{3}$$

$$T = \frac{T_{cc}}{[1+\frac{(\gamma-1)}{2}M^2]} \tag{4}$$

The heat transfer from combustion products to wall material should be determined which occurs by forced convection. Near the wall, gas delivers energy at stagnant condition in the boundary layer. Temperature of stagnant gas is called adiabatic wall temperature. Heat flux is computed with the equation (5).

$$q = h(T_{aw} - T_w) \tag{5}$$

Therefore, adiabatic wall temperature is needed which is obtained by the equation below.

$$T_{aw} = T_{cc}\left(\frac{1+r\frac{\gamma-1}{2}M_x^2}{1+\frac{\gamma-1}{2}M_x^2}\right) \quad \begin{matrix} r = Pr^{0.5} & \text{for laminar flows} \\ r = Pr^{0.33} & \text{for turbulent flows} \end{matrix} \tag{6}$$

Combustion chamber gas properties are obtained from inlet mass fractions from equation (7). Molecular weight of gas mixture is obtained from equation (8).

$$C_p = \sum_i Y_i C_{p,i} \tag{7}$$

$$MW = \sum_i \frac{Y_i}{MW_i} \tag{8}$$

Ratio of specific heats can be gathered from the equation (9)

$$\gamma = \frac{C_p}{C_p - R} \tag{9}$$

Viscosity of the chamber mixture can be calculated from equation (4) whereas Prandtl number can be found from equation (5) [Bartz, 1957]

$$\mu_0 = 1.81 \times 10^{-7} \times MW^{0.5} \times T_{cc}^{0.6} \tag{10}$$

$$Pr = 4\gamma/(9\gamma - 5) \tag{11}$$

Finally, c* can be computed from equation (12) and required inputs can be used.

$$c^* = \frac{\sqrt{\gamma R T_0}}{\gamma(\frac{2}{\gamma+1})^{\frac{\gamma+1}{2(\gamma-1)}}} \tag{12}$$

Convective heat flux is calculated using Bartz Method [Bartz, 1957; Bartz, 1965] which is a rapid estimation approach to determine heat transfer coefficients.

$$h = \left[\frac{C}{{D_{thr}}^{0.2}}\left(\frac{D_{thr}}{R_{c,th}}\right)^{0.1} \frac{\mu_0^{0.2} C_p}{Pr^{0.6}}\left(\frac{P_{cc}}{c^*}\right)^{0.8}\right](\frac{A_{thr}}{A})^{0.9}\sigma \tag{13}$$

where

$$\sigma = \frac{1}{[\frac{1}{2}\frac{T_w}{T_0}\left(1 + \frac{\gamma-1}{2}M^2\right) + \frac{1}{2}]^{0.8\frac{w}{5}} + (1 + \frac{\gamma-1}{2}M^2)^{w/5}} \tag{14}$$

- C is a constant (generally 0.026),
- $\mathrm{D_{thr}}$ is the diameter of the throat,
- $R_{c,th}$ is the convergent radius of the throat region,
- μ_0 is viscosity of the chamber gases,
- C_p is the specific heat capacity of the chamber gases,
- Pr is Prandtl number,
- P_{cc} is the combustion chamber pressure,
- c^* is the characteristic velocity,
- A_{thr} is throat area,
- T_0 is stagnation temperature.

The terms in square brackets are constant since they are chamber parameters. Other parameters such as

- A is the area of the specified location,
- M is the local Mach number,
- T_w is the temperature at the gas side of the wall,
- σ is the boundary layer correction for the nozzle location

depend on the location of the nozzle. With the Bartz Estimation, convection heat transfer coefficient is obtained for the nozzle.

Blowing Correction

Due to ablation of insulation material, mass injection of reaction products occur which decreases the convection heat transfer in the boundary layer. In addition, the injected mass contains reaction products which alter the species concentrations near wall. Therefore, it changes the heterogenous reactant composition and consequently product composition near the wall. Stanton number correction is used to include this reduction for the heat transfer calculations. Stanton number expresses the ratio of heat transfer of the fluid to heat capacity of the fluid.

$$C_H = \frac{h}{C_p \rho_\infty u_\infty} \tag{15}$$

To apply the correction mentioned above, following equation is used [Moyer and Wool, 1970].

$$C_H = C_{H1} \frac{\ln\left(1 + \frac{\dot{m}}{\rho_\infty u_\infty C_{H1}}\right)}{\dot{m}/\rho_\infty u_\infty C_{H1}} \tag{16}$$

Surface Mass Balances

Surface mass balances for species are modelled as described in [Ruffin, 2015] and it is shown in figure 2.

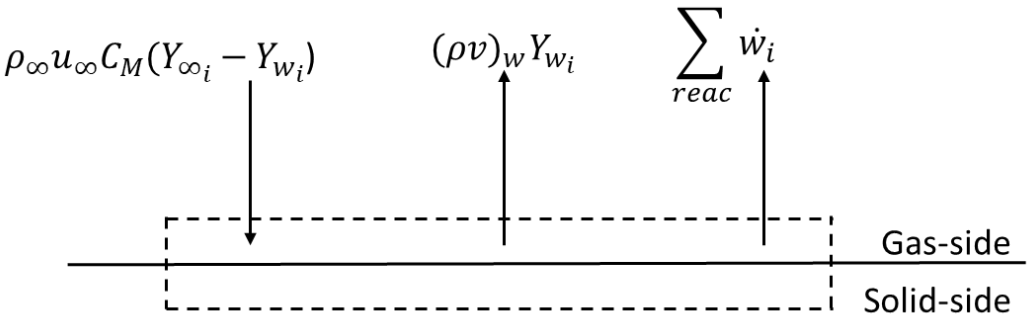

Figure 2: Surface Mass Balances

$$\rho_\infty u_\infty C_M \left(Y_{\infty_i} - Y_{w_i}\right) = (\rho v)_w Y_{w_i} + \sum \dot{w}_i \tag{17}$$

- ρ_∞ is free-stream density of the combustion gases,
- u_∞ is free-stream velocity of the combustion gases,
- C_M is mass transfer coefficient,
- $(\rho v)_w$ is the mass injection to gas-side due to ablation of TPS material,
- Y_∞ and Y_w are freestream and wall mass fractions respectively,
- $\dot{w}$ is the reaction rate.

i is the oxidizing species such as H_2O, CO_2. In order to get mass transfer coefficient Chilton-Colburn Analogy is employed to relate Stanton number for heat transfer to mass transfer.

$$C_H = C_M Le^{2/3} \tag{17}$$

For Le close to unity, one can assume that

$$C_H = C_M \tag{18}$$

Surface Heat Balance

After mass balance equations are iterated for each oxidizing species, surface heat balance is iterated to obtain wall temperature with the erosion rate. Heat sink effect of insulation material is neglected with the steady-state assumption. Therefore, conduction term in the heat transfer equation becomes

$$q_{conduction} = \rho_c C_{p_c} \dot{s}(T_w - T_0) \tag{20}$$

- $\boldsymbol{\rho_c}$ is density of the insulation,
- $\boldsymbol{C_{p_c}}$ is heat capacity of insulation,
- $\boldsymbol{\dot{s}}$ is the erosion rate,
- $\boldsymbol{T_w}$ and $\boldsymbol{T_0}$ is the wall and initial temperature respectively.

Surface heat balance is obtained from the equation below assuming radiation heat transfer is negligible.

$$q_{convection} = q_{conduction} + q_{chem} \tag{21}$$

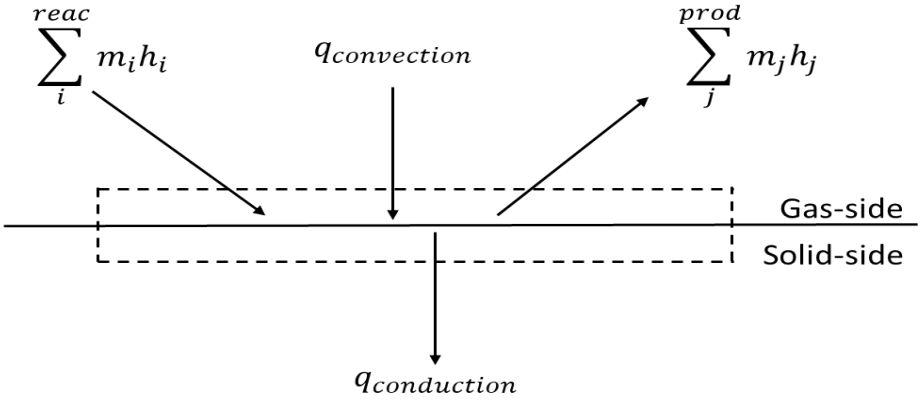

Figure 3: Surface Heat Balance

Chemical heat flux can be obtained from equation below.

$$q_{chem} = \sum_{i} \left(\sum_{prod} \frac{MW_{prod}}{MW_C} \frac{v_{prod}}{v_C} \int_{T^\circ}^{T_w} C_p \, dT + \Delta H^\circ_{reac} - \sum_{reac} \frac{MW_{reac}}{MW_C} \frac{v_{reac}}{v_C} \int_{T^\circ}^{T_w} C_p \, dT \right) \dot{m} \quad (22)$$

- MW is the molecular weight of reactants or products,
- v is the stoichiometric coefficients of reactants or products,
- C_p is the heat capacity of reactants or products,
- ΔH°_{reac} is the heat of reactions.

Heterogenous reactions are modelled with Arrhenius type equations from [Bianchi, Nasuti and Onofri, 2011] given in the table 1 with equations (23) and (24). Reaction rates are linked to mass transfer with stoichiometric coefficients and molecular weights shown in equation (22). Finally, the code gives the results for ablation mass and erosion rate from equations (25) and (26).

Table 1. Heterogenous reaction rate constants for H2O and CO2

Surface reaction	j	A_j	E_j,kJ/mol	b_j	n_j	ΔH°_{reac},MJ/kg
$C_{(s)} + H_2O \rightarrow CO + H_2$	1	480000	288	0	0.5	10.94
$C_{(s)} + CO_2 \rightarrow 2CO$	2	9000	285	0	0.5	14.37

$$k_j = A_j T_w^{b_j} exp\left(-\frac{E_j}{RT_w}\right) \quad (23)$$

$$\dot{m}_i = k_j P_i^{n_j} \quad (24)$$

$$\dot{m} = \dot{m}_{H2O} + \dot{m}_{CO2} \quad (25)$$

$$\dot{s} = \frac{\dot{m}}{\rho_C} \quad (26)$$

Similar solution algorithm is constructed as described in [Ruffin, 2015] to perform iterations for surface mass balances with surface heat balance. Surface mass balances embedded into surface heat balance loop. Therefore, to get convergence for surface heat balance, surface mass balances must be satisfied first. Surface mass balances for considered oxidizing species are iterated to get concentration of each oxidizing specie near wall with gradual corrections for every loop. When the iteration loop stops, concentration of every specie with their contribution to surface ablation is achieved. After convergence is obtained for both surface heat balance and mass balances, sigma correction factor is calculated again for Bartz Estimation. Also, blowing correction for heat transfer coefficient is corrected which reduces the heat transfer. Again, surface heat balance and surface balances are iterated with more accurate inputs. Results for erosion and wall temperature are gathered along nozzle axis.

RESULTS

Results from the developed code is compared with experimental data from the BAllistic Test and Evaluation System (BATES) motor firings conducted by Geisler using propellants with different aluminium contents [Geisler and Beckman, 1998]. The measurements of nozzle recession are only available for throat section which is the most critical region for motor performance. Therefore, another conformation necessity for erosion rate through the nozzle axis is answered by CFD simulations conducted by [Bianchi, Nasuti and Onofri, 2011] for the same cases for a Modified 70-lb BATES Nozzle Contour. Parameters of Modified 70-lb BATES Nozzle are given in table 2. Selected points to perform calculations on the nozzle contour are plotted in figure 4. Mach number and pressure are obtained with isentropic relations which are given in figure 5 and 6.

Table 2. Modified 70-lb BATES Motor Nozzle Parameters

Throat diameter	5.08 cm
Convergence half-angle	45°
Upstream throat radius	4.064 cm
Downstream throat radius	5.08 cm
Divergence angle	15°
Expansion ratio	10.2
Graphite density	1830 kg/m^3

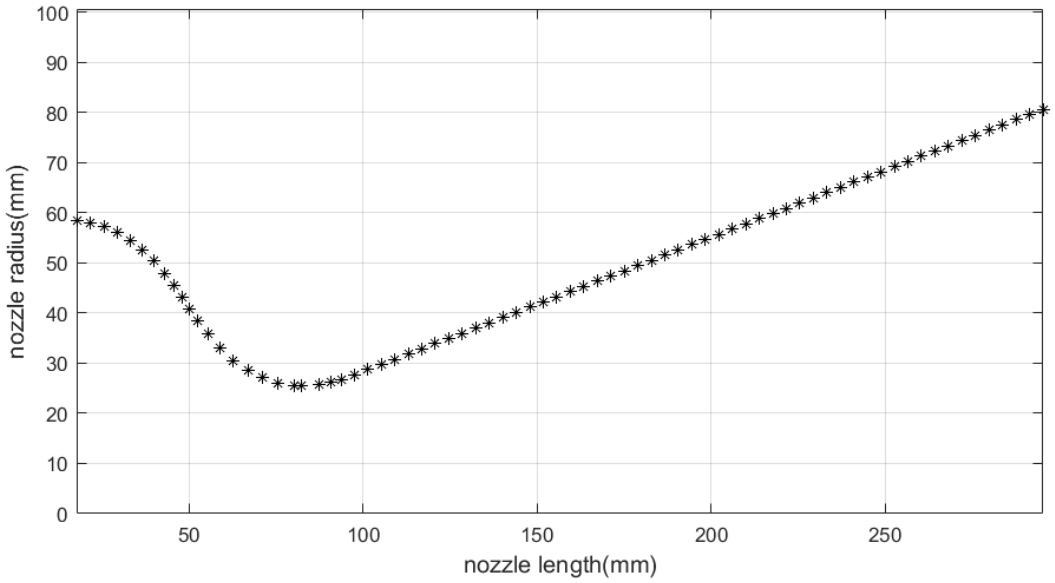

Figure 4: Calculation points on Modified 70 lb BATES motor nozzle contour

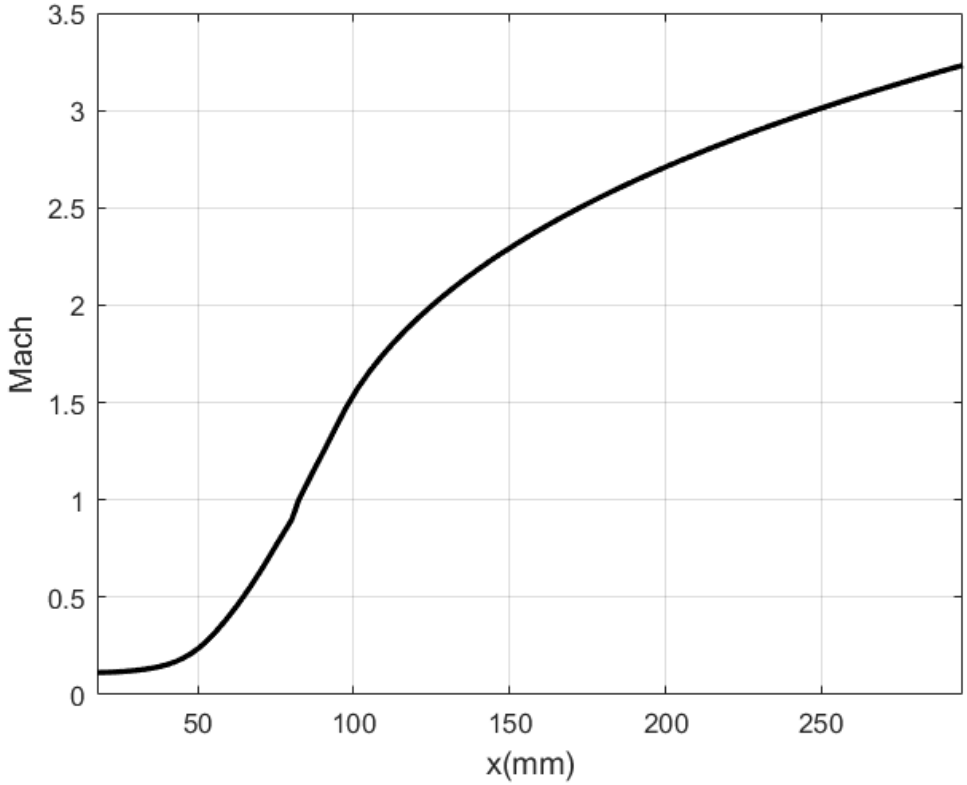

Figure 5: Mach number variation along nozzle axis

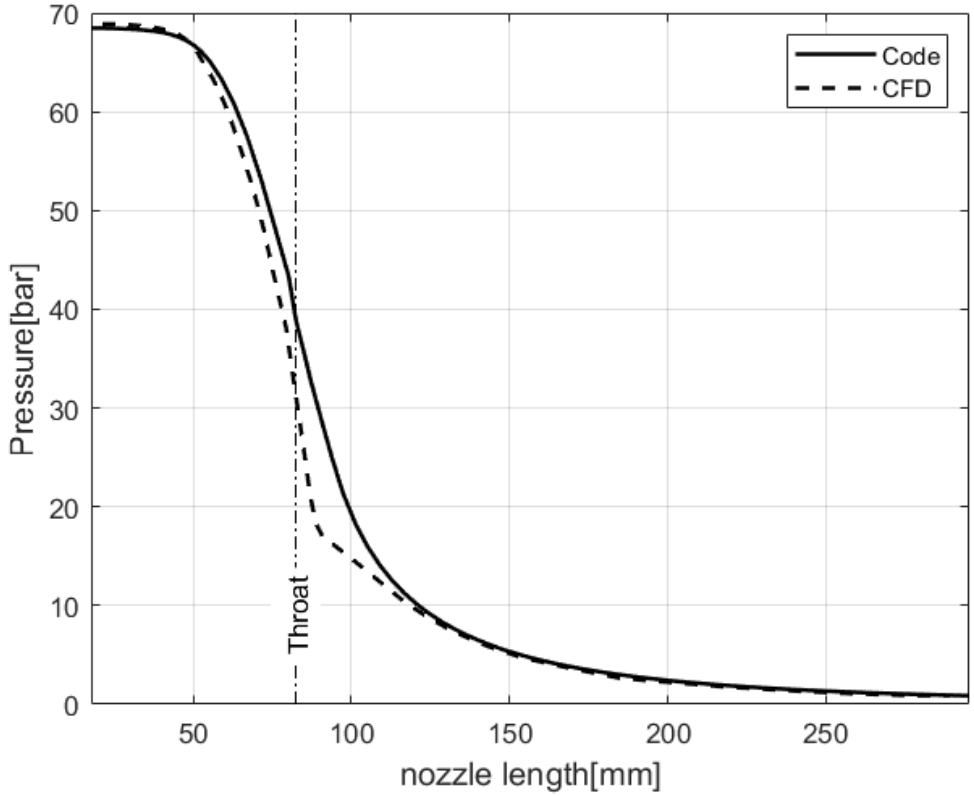

Figure 6: Pressure variation along nozzle axis with the developed code and CFD results from [Bianchi, Nasuti and Onofri, 2011]

Modified BATES 70 lb nozzle contour is used to calculate erosion rates on the nozzle surface. Input variables are gathered from the experiments conducted by Geisler for BATES motors given in [Bianchi, Nasuti and Onofri, 2011; Bianchi, Nasuti and Martelli, 2009; Geisler and Beckman, 1989]. Results from the code are compared with throat recession measurements from Geisler and CFD results from Bianchi. Input data for the nozzle inlet conditions are given in table 3.

Table 3. Mass fractions, pressure, temperature and aluminum content for inlet conditions of the experiments conducted by Geisler

Y_{CO}	Y_{CO2}	Y_{HCL}	Y_{H2}	Y_{H2O}	Y_{N2}	Y_{AL2O3}	Pc,bar	Tc,K	Al,%
0.175	0.04	0.24	0.02	0.145	0.1	0.28	69	3580	15
0.18	0.025	0.23	0.02	0.105	0.1	0.34	69	3655	18
0.20	0.015	0.195	0.02	0.07	0.1	0.40	69	3715	21
0.20	0.005	0.19	0.02	0.045	0.1	0.44	69	3750	24
0.20	0.005	0.19	0.02	0.025	0.1	0.46	69	3745	27

Figure 7 shows that preliminary estimation code gives reasonably accurate results for downstream of the throat and divergent nozzle part in terms of erosion. It can predict the erosion, and therefore can be beneficial estimation of the motor performance. However, it cannot predict erosion of converging part as well as diverging part.

On the other hand, wall temperature distribution closer to CFD results for the converging part. Difference in prediction of temperature increases from throat to exit of the nozzle as shown in figure 8. This is due to boundary layer growth for the diverging part of nozzle and accuracy of the code is limited by the accuracy of the Bartz estimation.

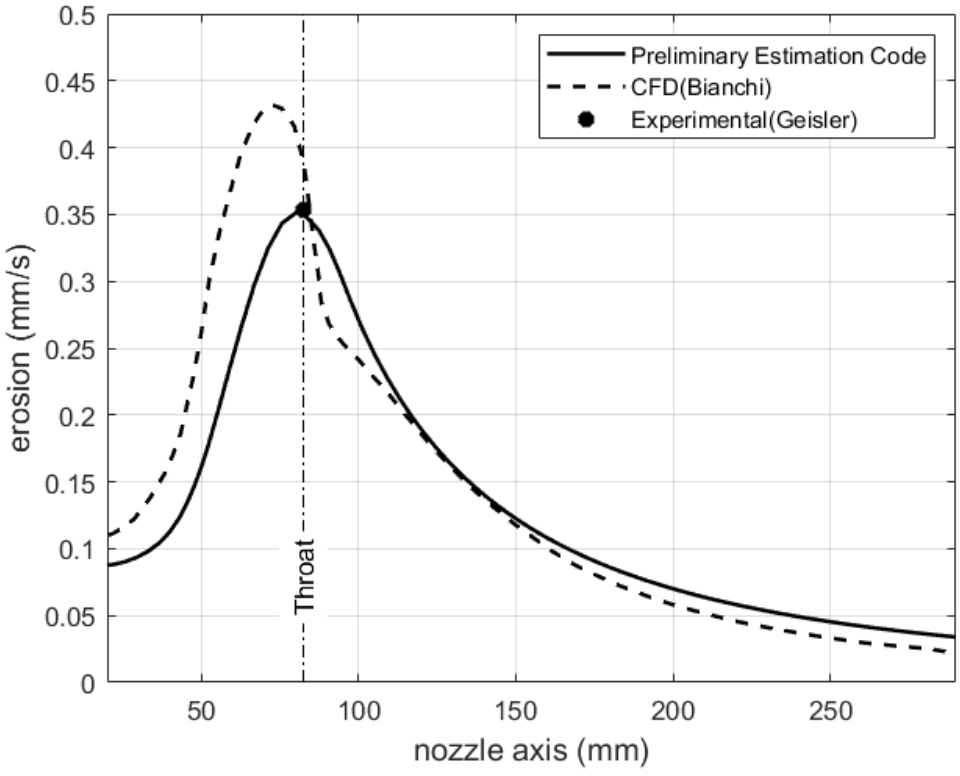

Figure 7: Erosion rate along the nozzle axis for the propellant with 15% aluminium content

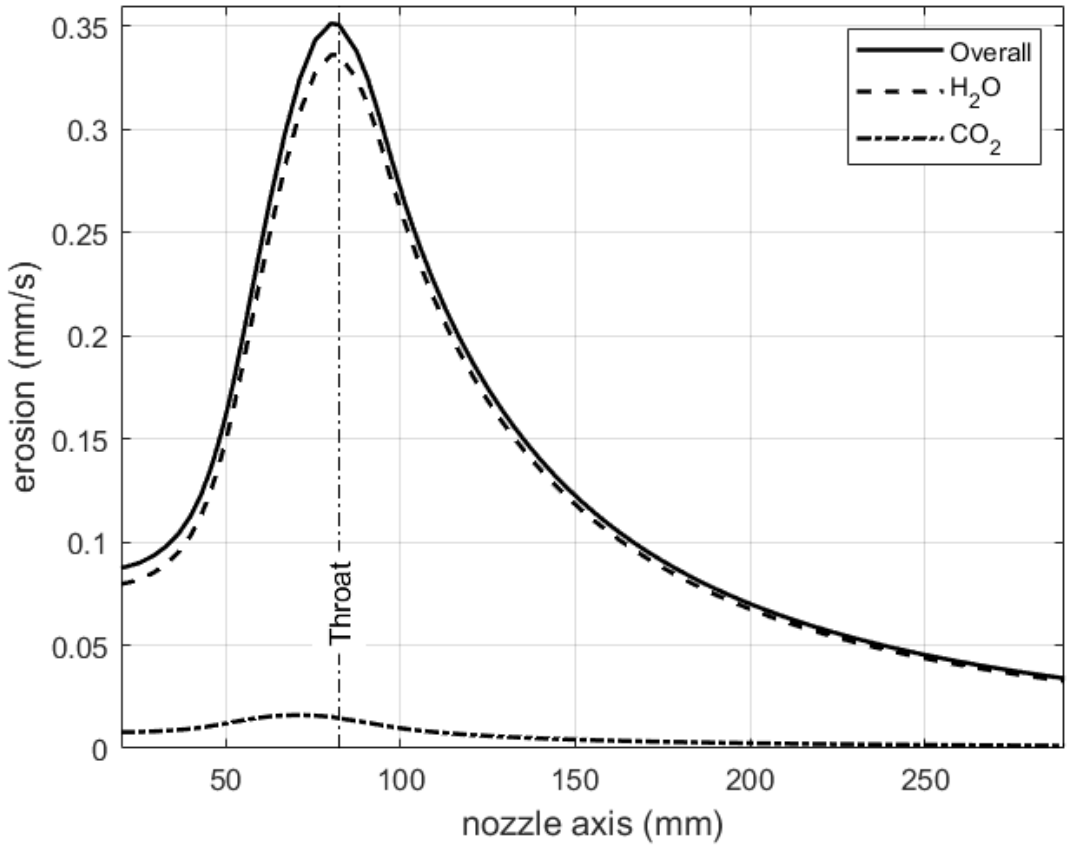

Figure 8: Oxidizing species effects on erosion for the propellant with 15% aluminium content

It is clear from the figure 8 that major contribution of the erosion can be attributed to water vapor. Also, contribution of CO_2 decreases for the divergent part of the nozzle due to pressure drop. Throat recession drops to a fifth of the propellant with 15% Aluminum content for propellant with 27% aluminium content due to lack of oxidizing species as shown in figure 9. The code underestimates the erosion on converging part and overestimates on diverging part. Very close results for convering wall temperature is obtained, but difference between CFD and Bartz Estimation increases as boundary layer grows for the diverging part of the nozzle as shown in figure 10.

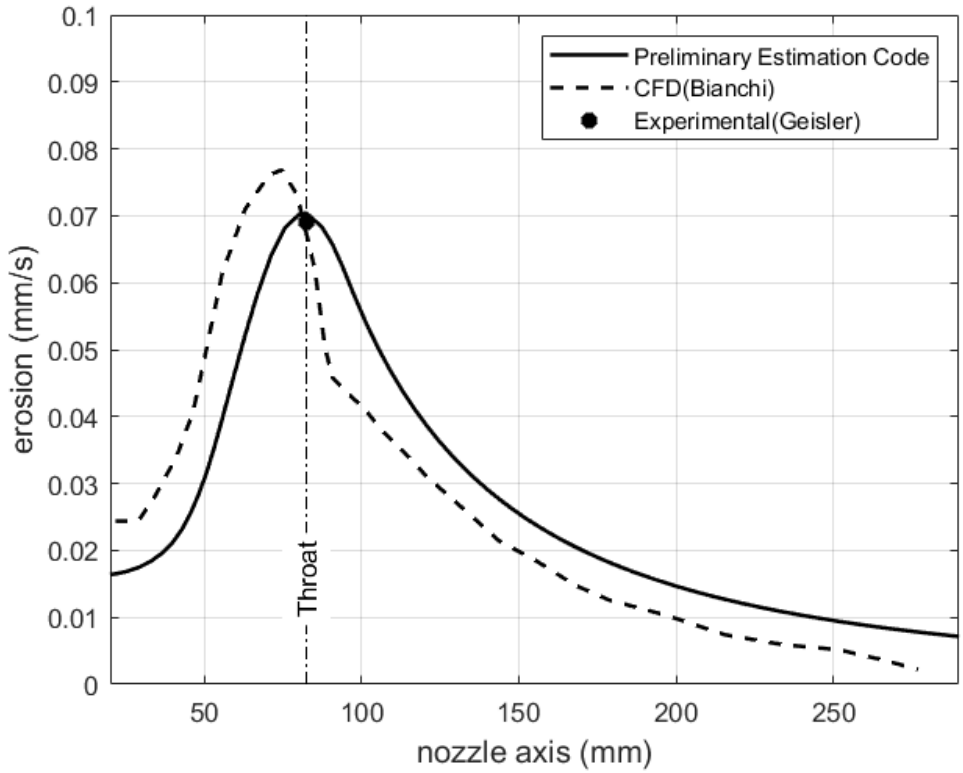

Figure 9: Erosion rate along the nozzle axis for the propellant with 27% aluminium content

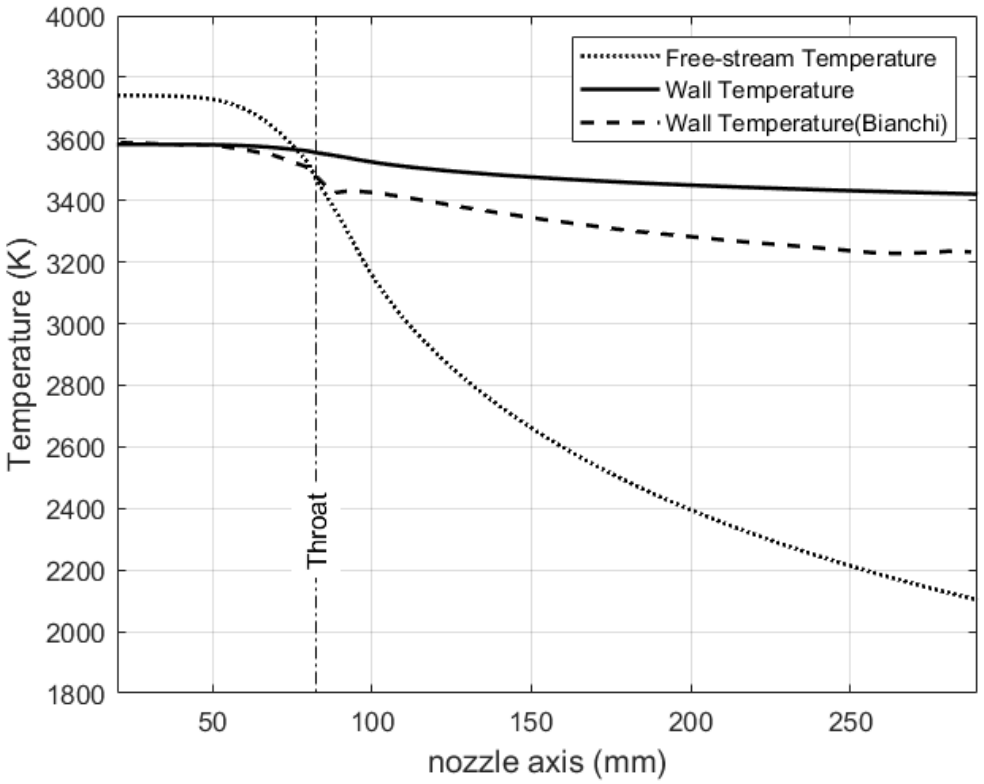

Figure 10: Free-stream and Wall Temperature along nozzle axis for the propellant with 27% aluminium content

Erosion rates for propelllant with different aluminium contents are given in figure 11. Although inlet temperature for the nozzle increases with aluminium content, erosion decreases. This due to increased mass fraction of Al_2O_3 which is modeled as inert gas. Oxidizing species concentrations reduce and erosion rates decrease as a consequence, since Al_2O_3 limits the existence of oxygen-atoms in oxidizing species. [Thakre, 2008]

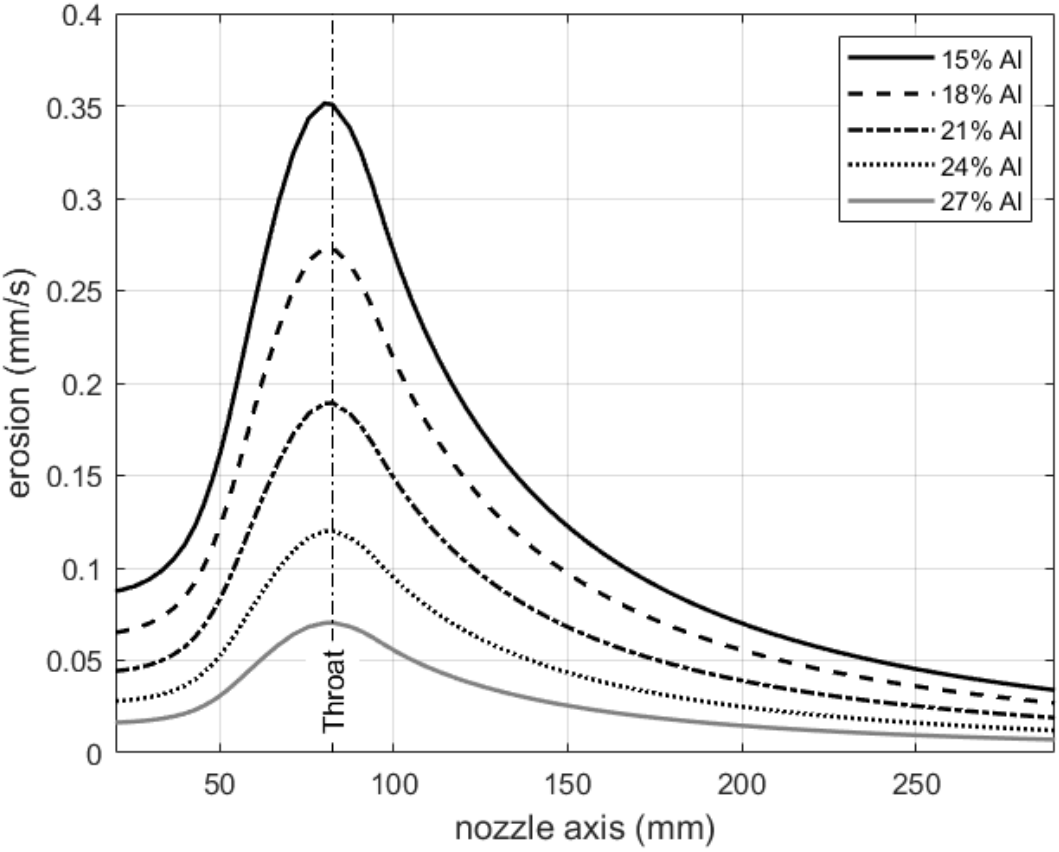

Figure 11: Erosion results for propellants with different aluminium content

Table 4. Comparison of erosion rates at throat

Al (%)	Thakre (mm/s)	Bianchi (mm/s)	Experimental (mm/s)	Code (mm/s)	Difference (%)
15	0.3370	0.3958	0.3531	0.3507	-0.68
18	0.2750	0.2907	0.2845	0.2734	-3.90
21	0.2070	0.1943	0.2000	0.1893	-5.35
24	0.1310	0.1226	0.1245	0.1201	-3.53
27	0.0760	0.0684	0.0686	0.0704	2.62

For diffusion limited cases such as metallized solid rocket motors, preliminary estimation code gives reliable results. Throat erosion can be estimated with a good accuracy and motor performance can be predicted during the operation. Temperature difference between CFD and

code is at most 10% for the divergent part of nozzle. For diverging part, the code overestimates both erosion and wall temperature. It can be used as a design tool since it leaves the calculations on the safe side. On the other hand, it can predict wall temperatures for the converging part, but underestimates erosion. Since pressure is higher and boundary layer is thinner, heat flux for converging section is higher which is underestimated with Bartz Estimation. In conclusion, developed program provides reasonably close results which can be beneficial for the preliminary thermal design phase of metallized solid propellant rocket motor nozzles in a matter of seconds.

References

Bartz, D.R. (1957) *A Simple Equation for Rapid Estimation of Rocket Nozzle Convective Heat Transfer Coefficients*, Journal of Jet Propulsion, Vol 27, p: 49-51, January 1957

Bartz, D.R. (1965) *Turbulent Boundary-Layer Heat Transfer from Rapidly Accelerating Flow of Rocket Combustion Gases and of Heated Air*, Advances in Heat Transfer. Vol 2, p:1-108, January 1965.

Bianchi, D., Nasuti, F. and Martelli, E. (2009) *Coupled Analysis of Flow and Surface Ablation in Carbon-Carbon Rocket Nozzles*. Journal of Spacecraft and Rockets, Vol 46, p: 492–500, May-June 2009.

Bianchi, D., Nasuti, F. and Onofri, M. (2011) *Thermochemical Erosion Analysis for Graphite/Carbon-Carbon Rocket Nozzles*, Journal of Propulsion and Power, Vol 27, p: 197–205, January-February 2011.

Borie, V., Brulard, J. and Lengellet, G (1989) *Aerothermochemical Analysis of Carbon-Carbon Nozzle Regression in Solid-Propellant Rocket Motors*, Vol 5, p: 665–673, November-December 1989.

Geisler, R. and Beckman, F. (1998) *The History of the BATES Motors at the Air Force Rocket Propulsion Laboratory*. 34th AIAA/ASME/SAE/ASEE Joint Propulsion Conference & Exhibit, July 1998, Cleveland, OH.

Kuo, K. K. and Acharya, R. (2012) Applications of Turbulent and Multiphase of Combustion, John Wiley & Sons, 2012.

Moyer, C. B. and Wool, M. R., (1970) User's Manual, Aerotherm Charring Material Thermal Response and Ablation Program, Version 3, Volume 1, Program Description and Sample Problems, Air Force Rocket Propulsion Laboratory, Edwards AFB, CA, April 1970.

Ruffin, A. (2015) Numerical Investigation of Nozzle Thermochemical Behaviour in Hybrid Rocket Motors, University of Padova, Venice, Italy.

Sutton, G. P. and Biblarz, O. (2001) Rocket Propulsion Elements. John Wiley & Sons, Inc., 2001.

Thakre, P. (2008) Chemical Erosion of Graphite and Refractory Metal Nozzles and Its Mitigation in Solid-Propellant Rocket Motors, The Pennsylvania State University, USA.